Journal of Materials Chemistry A

ROYAL SOCIETY OF CHEMISTRY

PAPER

View Article Online
View Journal | View Issue



Cite this: J. Mater. Chem. A, 2020, 8, 9629

# A novel integrated Cr(VI) adsorption–photoreduction system using MOF@polymer composite beads†

Bardiya Valizadeh, Tu N. Nguyen, ‡ Stavroula Kampouri, Daniel T. Sun, Mounir D. Mensi, Kyriakos Stylianou, Berend Smit and Wendy L. Queen *

Received 27th January 2020
Accepted 20th April 2020

DOI: 10.1039/d0ta01046d

rsc.li/materials-a



Herein, a novel integrated adsorption–photoreduction system, which captures highly mobile and toxic hexavalent chromium (Cr(VI)) from real-world water samples and reduces it to less mobile and benign Cr(III) species, was designed. To do this, a known Zr-MOF, UiO-66, was functionalized with double amino groups. This modification permits the new material, Zr-BDC-$(NH_2)_2$, to play a dual-purpose as both adsorbent and photocatalyst. Next, Zr-BDC-$(NH_2)_2$ was incorporated into MOF@polymer beads (M@PB) using polyethersulfone (PES) that was chemically modified with carboxylic acid groups to improve hydrophilicity. The modification enhances the Cr(VI) extraction rate of the beads by a factor of ~3 when compared to the unmodified counterpart. In addition, Zr-BDC-$(NH_2)_2$@PB offers one of the highest Cr(VI) uptake capacities reported to date, rapid extraction rates, high selectivity for Cr(VI) in real-world water samples, and full recyclability. The adsorption and subsequent regeneration cycles are carried out in a glass column equipped with a visible light source, demonstrating that the Cr(VI) concentration is brought below drinkable levels, and the Cr(VI) subsequently photoreduced to Cr(III) species using light irradiation during adsorbent regeneration. To the best of our knowledge, this is the first demonstration of MOF-based adsorption–photoreduction of Cr(VI) in a single process.

## 1. Introduction

Providing access to clean water is seen as one of the main challenges of our generation.[1] In this context, the development of energy efficient processes able to rapidly remove water contaminants plays an important role in both the water-energy nexus and our effort to globally improve human health and environmental well-being.[2] Given this, the title work is focused on reducing chromium contamination, which is particularly problematic in many regions throughout the world.[3] Chromium is commonly found in two oxidation states, trivalent, Cr(III), and hexavalent, Cr(VI), and the toxicity of chromium depends on the oxidation state; Cr(VI) anions, including $CrO_4^{2-}$ and $Cr_2O_7^{2-}$, are known carcinogens. Because these Cr(VI) anions are highly mobile in water, the contaminants, which are often released from leather, textile, cement, dye, glass and steel manufacturing industries, can readily end-up in surface and ground water.[4] Cr(III), however, is far less mobile and only toxic at high concentrations. In fact, it has been suggested that trace amounts of Cr(III) are essential to both humans and the metabolic system of many plants.[5] Due to the serious toxicity of Cr(VI) and the difficulty in differentiation between the two oxidation states using standard methods for water analysis, the total Cr concentration in drinking water is strictly limited to 100 ppb by the U.S. Environmental Protection Agency (EPA) and 50 ppb by the World Health Organization (WHO).[6–8]

To date, the main methods for Cr(VI) removal from water are chemical precipitation or chemical/photoreduction.[9] Both methods are less effective at low concentrations, and chemical precipitation, although simple and inexpensive, produces large amounts of sludge and solid waste.[10,11] Chemical- or photoreduction often results in high concentration of Cr(III) in water streams, and, as such, demands a secondary treatment method to reduce concentrations below what is deemed acceptable by the EPA or WHO.[12] Therefore, an active area of research is to replace these conventional technologies by solid adsorption, in which the aim is to identify selective materials that are highly effective at low concentrations.[13]

Some adsorbent-based technologies have already been developed for Cr removal. Most of these technologies use low-cost bio-waste adsorbents and ion-exchange resins. The solid waste from several agricultural or industrial processes, such as chitosan and coconut shells, can be used for Cr capture.[14] Although cost-effective, they are sensitive to operating

*Institut des Sciences et Ingénierie Chimiques, Valais, Ecole Polytechnique Fédérale de Lausanne (EPFL), Rue de l'Industrie 17, CH-1951 Sion, Switzerland. E-mail: wendy.queen@epfl.ch*

† Electronic supplementary information (ESI) available: Experimental details. See DOI: 10.1039/d0ta01046d

‡ Current address: Helen Scientific Research and Technological Development Co., Ltd., Ho Chi Minh City, Vietnam.

conditions, such as pH, and typically offer low adsorption capacity and selectivity.[15] Commercially available resins, such as layered double hydroxides and amino-containing organic resins, are relatively expensive and suffer from poor recyclability and thermal and chemical stability.[13] These limitations, drive scientific efforts aimed at the design of new adsorbent technologies. One highly active area of research is in the field of metal–organic frameworks (MOFs), a class of materials which offer permanent porosity, a large number of highly diverse structure types, and unmatched chemical tunability.[16,17] Several recent reports demonstrate that MOFs can have superior capacity and selectivity for Cr(VI) in aqueous solutions than the aforementioned adsorbents.[18–20] However, the state of the art MOF-based adsorption systems often create highly toxic Cr(VI) waste that is still complicated to treat and dispose.

It is thought that an ideal process involves a combination of adsorption and reduction. The adsorption is required to reduce Cr concentration in the effluent below drinkable limits and the reduction enables the conversion of Cr(VI) into Cr(III), resulting in much less toxic waste after adsorbent regeneration. Although there are some polyaniline-based composite adsorbents that can chemically reduce Cr(VI),[21,22] in this work, we develop a process that is based on a MOF that simultaneously and selectively adsorbs chromium ions and photo-reduces the toxic Cr(VI) into the less harmful Cr(III). We show that this MOF can be incorporated into MOF@polymer composite beads, which has one of the highest capacities for Cr(VI) reported to date. In addition, using an adsorption–photoreduction column, we show that our system not only reduces Cr(VI) to below drinkable concentrations, but also reduces it to the less toxic and less mobile Cr(III). As such, there is no need for any treatment upon adsorbent regeneration and chromium release.

## 2. Process design

The reported process was developed in three steps. First, a MOF that can selectively adsorb and photoreduce Cr(VI) was designed. Next, the MOF powder was incorporated into MOF@polymer composite beads, and finally, the beads were placed in a column equipped with a light source to demonstrate the extraction/photoreduction of Cr(VI) from distilled and river water.

### 2.1. MOF design

Our aim is to design a MOF that can selectively adsorb and photoreduce Cr(VI) to Cr(III). Interestingly, several MOFs have been reported for selective Cr adsorption[23,24] and several MOFs have also been studied in catalytic amounts for the photoreduction of Cr(VI).[12,25] Despite this, to the best of our knowledge, no MOFs are reported that combine both functionalities in a single process. Among these, amine ($NH_2$)-functionalized MOFs are known to be efficient photocatalysts due to their absorption band in the visible region.[26–29] In addition, $NH_2$-functionalized MOFs can also promote the ion-exchange of Cr(VI); in such studies, the $NH_2$ group reportedly plays a vital role in the adsorption of chromium ions, after protonation of the amine with HCl.[19,30] Since the extraction is carried out in aqueous solutions, it is essential to have a water-stable MOF. Among these $NH_2$-functionalized MOFs, UiO-66 was selected for this study as it reportedly has excellent water stability.[31] The UiO-66 structure type consists of $[Zr_6(\mu_3\text{-}O)_4(\mu_3\text{-}OH)_4]^{12-}$ nodes that are interlinked by 1,4-benzenedicarboxylate ($BDC^{2-}$) ligands. Here, we show that this structure type can be synthesized with double-$NH_2$ functionality on the $BDC^{2-}$ ligands,[32] which enhances both the chromium extraction as well as the photocatalytic activity.

The details of the synthesis and characterization of UiO-66 containing ligands functionalized with two amine groups (hereafter referred to as Zr-BDC-$(NH_2)_2$) are described in the ESI.† While Zr-BDC-$(NH_2)_2$ has the same cubic crystal structure as UiO-66 (space group $Fm\bar{3}m$, $a$-axis 20.8112(3) Å, Fig. S1†), the additional $NH_2$ functionality increases the Cr(VI) adsorption capacity by approximately 10% compared to its mono-aminated counterpart (see Table 1). It is thought that this additional functionality increases the number of adsorption sites but decreases the available pore volume from 0.65–0.7 to 0.2 $cm^2\ g^{-1}$ for UiO-66 (ref. 33 and 34) and Zr-BDC-$(NH_2)_2$, respectively; the net result is only a slight increase of capacity. A more significant effect is observed for the light adsorption. The UV-vis absorbance spectrum of Zr-BDC-$(NH_2)_2$ demonstrates a significant red shift compared to the mono-aminated UiO-66 and a much broader absorption over the visible range (Fig. S2†).

### 2.2. MOF@polymer composite

After the synthesis of Zr-BDC-$(NH_2)_2$, which offers an enhancement in both the adsorption capacity for chromium and light-harvesting properties, we aimed to implement this material in an adsorption column. However, applying nano/micro-scale MOF powder directly into columns is often challenging due to issues regarding clogging, pressure drop, and material loss. To address these issues, the MOFs were embedded into a polymer matrix to form MOF@polymer composite beads (M@PB).[35] However, careful selection of the polymer is required, as this component can enhance or diminish performance. Given that the desired application is based on separations from water, one would like to ensure that the polymer is sufficiently hydrophilic. As such, polyethersulfone (PES) was selected and subsequently modified with carboxylic groups, which can enhance hydrophilicity. A comparison between un-modified and modified PES indicates a significant decrease in the water contact angle from 89° to 25°, respectively (Fig. S4†).

Zr-BDC-$(NH_2)_2$@PBs were synthesized with 80 wt% loading of Zr-BDC-$(NH_2)_2$ and modified PES blend. The powder X-ray diffraction (PXRD) patterns show that Zr-BDC-$(NH_2)_2$ crystals remain intact (Fig. S1†). Moreover, energy-dispersive X-ray spectroscopy (EDX) shows a homogeneous loading of the MOF in the polymer matrix (Fig. 3). From a practical point of view, it is important that the polymer matrix does not prevent the adsorption of guest molecules by blocking the pore entrance and/or filling the pores. The BET surface areas, which were calculated from $N_2$ isotherms at 77 K, are 402 and 372 $m^2\ g^{-1}$ for Zr-BDC-$(NH_2)_2$ and Zr-BDC-$(NH_2)_2$@PB, respectively (Fig. S3†).

 

Table 1 Sorption capacities for chromium species by MOF-based sorbents in the literature

| Sorbent | Capacity (mg $g^{-1}$ adsorbent) | | | Equilibrium time | Recyclability (% in # cycles) | Ref. |
|---|---|---|---|---|---|---|
| | Cr(VI) | $CrO_4^{2-}$ | $Cr_2O_7^{2-}$ | | | |
| UiO-66-$NH_2$@silica | 133.4 | — | 277.4 | 30 min | 8 cycles | 24 |
| UiO-66-$NH_2$@algenic acid (MOR-1-HA) | 135[a] | — | 280 | 9 min | 5 cycles | 19 |
| UiO-66-$NH_2$ (MOR-1) | 119[a] | | 247 | >10 min | — | 30 |
| UiO-66 | 62[a] | | 129 | — | — | 30 |
| $Zn_{0.5}Co_{0.5}$-SLUG-35 | 30.7[a] | 68.5 | — | 4 h | — | 37 |
| BUT-39 | 104[a] | — | 215 | 1 min | 90% in 3 cycles | 23 |
| JLU-MOF60 | 72[a] | — | 149 | 10 min | 4 cycles | 25 |
| SLUG-21 | 26.9[a] | 60.1 | — | 48 h | — | 38 |
| 1-$ClO_4$ | 28.2 | 62.9 | — | 6 h | — | 39 |
| FIR-53 | 35.7[a] | — | 74.2 | 4 h | 87% in 5 cycles | 40 |
| FIR-54 | 49.6[a] | — | 103 | — | 63% in 5 cycles | 40 |
| ABT·2$ClO_4$ | 103[a] | — | — | 24 h | NA | 41 |
| MONT-1 | 102[a] | — | 211.8 | 24 h | 73% in 5 cycles | 42 |
| 2D-Ag-3 | 80[a] | — | — | 24 h | NA | 43 |
| ZJU-101 | 118[a] | — | 245 | — | NA | 18 |
| 1-$SO_4$ | 80[a] | — | 166 | 72 h | — | 44 |
| **Zr-BDC-$(NH_2)_2$** | **146** | **—** | **303** | **16 min** | **5 cycles** | **This work** |
| **Zr-BDC-$(NH_2)_2$@PB** | **208** | **—** | **432** | **35 min** | **5 cycles** | **This work** |

[a] Calculated from reported value.



A typical value of the BET for the neat polymer beads is 12 $m^2$ $g^{-1}$, hence if we assume no polymer–MOF interference we would expect a BET of $402 \times 0.8 + 12 \times 0.2 = 324$ $m^2$ $g^{-1}$. The fact that the composite beads have a higher BET surface area indicates that there is some synergy between the MOF and the polymer at the interface. For more detail on the synthesis and characterization see the ESI.†

## 3. Adsorption thermodynamics and kinetics

As the next step, the extraction capacity of Cr(VI) was measured by soaking Zr-BDC-$(NH_2)_2$ and Zr-BDC-$(NH_2)_2$@PB in aqueous solutions containing various concentrations of $Cr_2O_7^{2-}$. The amount of adsorbed Cr(VI) was calculated by subtracting the final chromium concentration from the initial one. An enhancement in the Cr(VI) capacity, by ~42%, is observed (Fig. 1(a)) when going from the MOF to M@PB. It is hypothesized that there are synergistic effects between the MOF and polymer, which might promote the formation of molecular pockets in the polymer matrix at the MOF–polymer interface; the latter could introduce new adsorption sites within the polymer matrix.[35,36] Despite this, the MOF and M@PB exhibit similar capacities at low concentrations indicating that the amines are likely responsible for the materials performance in this concentration regime. It is also noted that the neat PES polymer beads have negligible Cr(VI) uptake (Fig. 1(b)); this indicates that the capacity of Zr-BDC-$(NH_2)_2$@PB is indeed attributed to the Zr-BDC-$(NH_2)_2$ crystals and the aforementioned synergy created between the MOF and polymer at the interface of the two dissimilar components. Last, EDX analysis of Zr-BDC-$(NH_2)_2$@PB saturated with Cr(VI) showed less than 2 wt% of un-exchanged $Cl^-$; this indicates that there are few remaining adsorption sites (Fig. S7†).

It is interesting to compare the Cr(VI) extraction capacity of Zr-BDC-$(NH_2)_2$@PB to state of the art materials reported in the literature. It should be noted that since the Cr(VI) capacity is determined using different anions in aqueous solution, in Table 1 we converted all reported data into mg Cr(VI) per g of sorbent. To the best of our knowledge, our materials have the highest Cr(VI) sorption capacities among MOF-based ion exchangers and adsorbents reported to date. However, some non-MOF-based technologies have been reported with higher capacities (see Table S2†).

For water treatment, the Cr(VI) capture at low ppm levels is crucial. Firstly, simple batch experiments were performed to determine the differences in efficiency in capturing $Cr_2O_7^{2-}$ at low concentrations. In these experiments, 50 mg of adsorbent was added to 5 mL of contaminated water at a concentration of 5 ppm Cr(VI) and a pH ~ 3, which is typical of industrial wastewater streams.[45] As expected, Fig. 1(b) shows that the Zr-BDC-$(NH_2)_2$@PB composite again has enhanced Cr(VI) removal when compared to Zr-BDC-$(NH_2)_2$ despite having 20% less MOF inside the composite. Considering that the neat polymer has negligible contribution to the Cr(VI) removal, this again indicates that there is some synergy between the MOF and polymer that lends to enhanced extraction even at low concentrations. Next, it was necessary to see if the material is capable of getting solutions below the EPA and WHO standard limit of 100 and 50 ppb, respectively (Fig. 1(c)). For this, Zr-BDC-$(NH_2)_2$@PB was placed in 500, and 200 ppb Cr(VI) solutions. After 24 hours, the composite was removed and analysis of the resulting solution indicated that chromium is indeed below the desired concentration. While the pH of the aforementioned solutions did not deviate from the starting pH ~ 3 upon treatment, a similar adsorption test was also performed in water, at pH = 7,

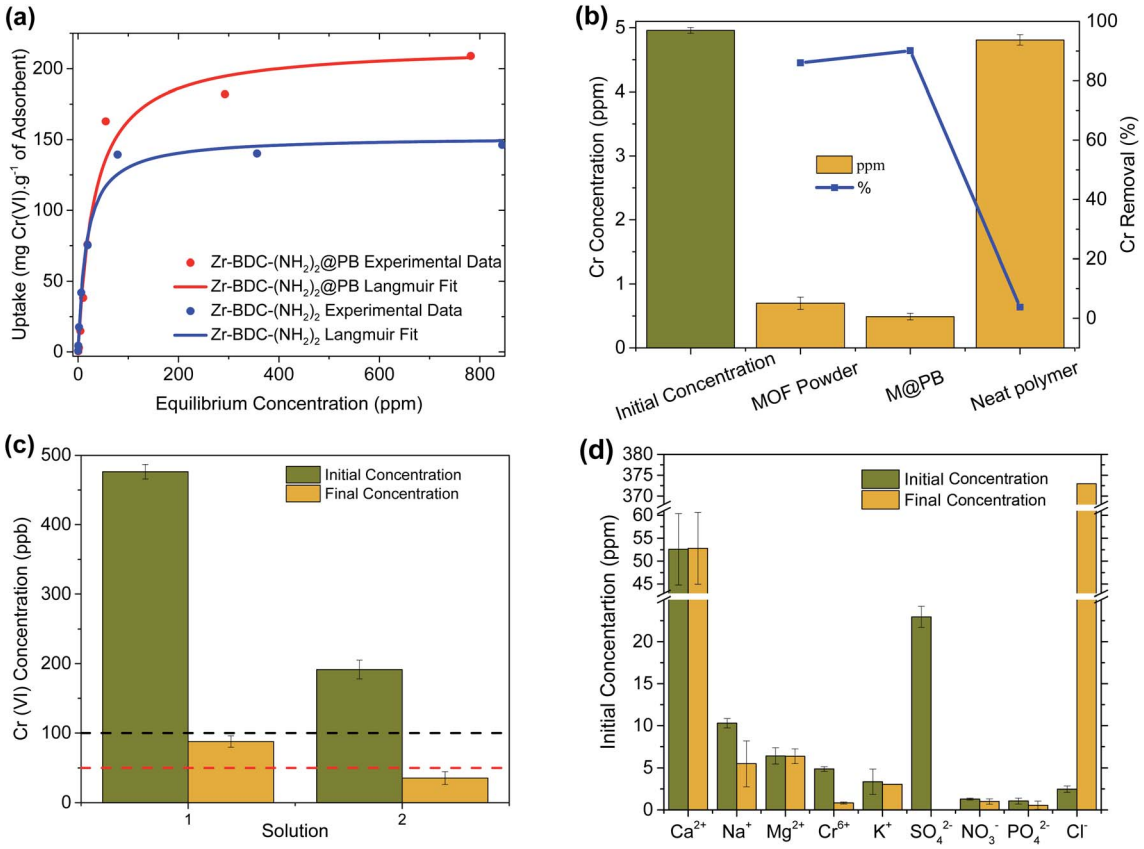


Fig. 1 (a) Equilibrium Cr(VI) sorption data for Zr-BDC-$(NH_2)_2$ powder and Zr-BDC-$(NH_2)_2$@PB. The solid lines represent the fitting of the data with the Langmuir model. (b) Cr(VI) removal ability of Zr-BDC-$(NH_2)_2$@PB *vs.* Zr-BDC-$(NH_2)_2$ powder and neat PES polymer beads at low concentration solutions (c) Zr-BDC-$(NH_2)_2$@PB removal ability to concentrations lower than standard limits (d) selectivity of Cr(VI) over ions present in Rhone river water.

containing 1 ppm Cr(VI). Expectedly, there is a slight decrease in the pH of the purified water after chromium removal, pH = 6 ± 0.1, a direct result of the acidic ion-exchange sites on the internal MOF surface.

Often waste water from various industries can run off into natural water streams, resulting in highly complex mixtures that contain a variety of competing organic and inorganic interferents which can affect the performance of the adsorbent. Hence, efforts were made to test Cr(VI) selectivity in surface water samples. For this, Zr-BDC-$(NH_2)_2$@PB was placed in the Rhone river (Sion, Switzerland) water sample that was spiked with 5 ppm Cr(VI). The resulting data, Fig. 1(d), shows no more than 7% change in the performance of Zr-BDC-$(NH_2)_2$@PB in the presence of various anions and cations found in river water. While this indicates that the material is an effective adsorbent, even in a complex real water media, there is also an indication that the material is adsorbing a noticeable amount of $SO_4^{2-}$, which could likely be responsible for the slight performance reduction.

Another crucial criterion for adsorbents is the rate of extraction, which determines the time required for each adsorption cycle. The kinetic experiment (Fig. 2(a)) shows that in less than 5 minutes, ~50% of the Cr(VI) is extracted, and in 35 min equilibrium was reached with more than 85% Cr(VI) removed. This is among the faster Cr(VI) extractions reported thus far in the literature (Table 1). Further, it is observed that the PES bead, modified with carboxylates, is faster to equilibrium (by a factor of ~3) and has a slightly higher extraction efficiency, when compared to the unmodified PES bead. This demonstrates that hydrophilic carboxylic acid groups, which allow for better water contact and diffusion into the Zr-BDC-$(NH_2)_2$@PB (Fig. S4†), is a method to improve material performance. This can also be confirmed by EDX mapping data showing the homogenous distribution of Cr in the Zr-BDC-$(NH_2)_2$@PB (Fig. 3). From a practical point of view, the rapid

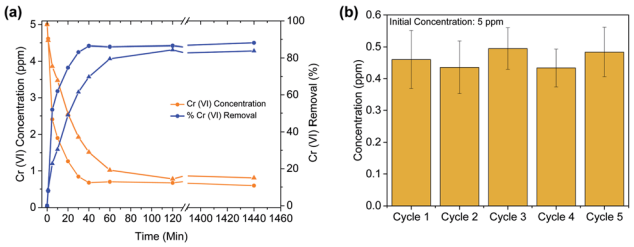


Fig. 2 (a) Kinetics of Cr(VI) adsorption for Zr-BDC-$(NH_2)_2$@PB, where the PES polymer is chemically modified with carboxylic acid groups (circle) and the unmodified PES (triangle) beads (b) Cr(VI) removal performance of Zr-BDC-$(NH_2)_2$@PB in five consecutive cycles.

 

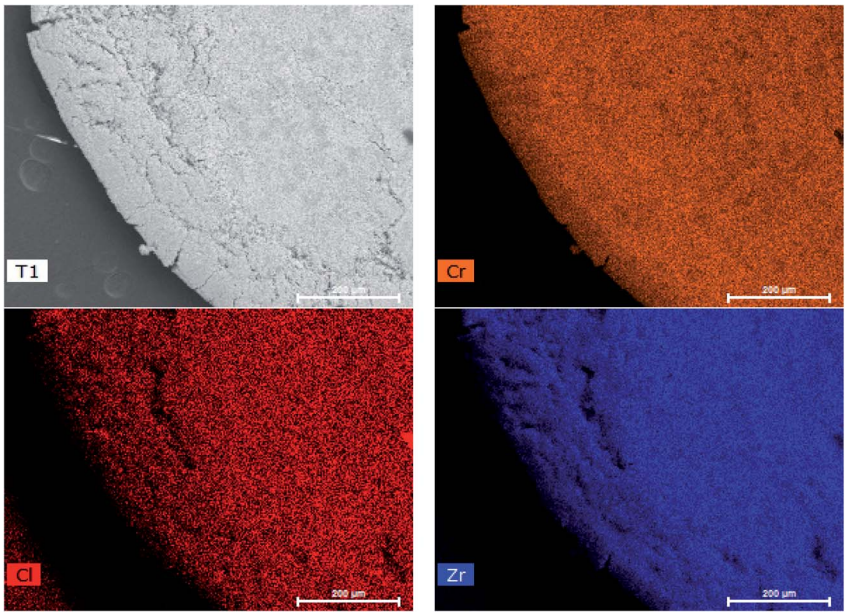


Fig. 3 EDX mapping of the cross section of a cut Zr-BDC-$(NH_2)_2$@PB after Cr capture.

capture of Cr(VI) will promote an adsorption system with high flow rates, where the liquid can have shorter contact time with the adsorbent.

## 4. Photoregeneration

To regenerate the Cr(VI) loaded Zr-BDC-$(NH_2)_2$@PB, we use a combination of photoreduction and ion exchange. To demonstrate regeneration, the beads were placed in an HCl solution that was illuminated with visible light *via* a Xe lamp; the former was meant to promote ion exchange, and the latter was meant to promote the reduction of Cr(VI) to Cr(III). This process was optimized by changing the pH and exposure time (see the ESI† for details). Once the procedure was optimized, Zr-BDC-$(NH_2)_2$@PB underwent extraction/regeneration cycles in batch experiments, carried out in an aqueous solution containing 5 ppm concentration of Cr(VI). Fig. 2(b) shows five consecutive sorption/regeneration cycles indicating complete recyclability of the Zr-BDC-$(NH_2)_2$@PB. Further, within error of our experiments, we see no signs of reduction in the composite's performance at the end of 5 cycles, indicating that the material has a potentially impressive lifetime.

From a practical point of view, it is not only important that we can regenerate our material; it is also important to ensure that there is no Cr(VI) in the solution after regeneration. As such, XPS analysis was used to monitor the oxidation state of chromium inside the fully loaded Zr-BDC-$(NH_2)_2$@PB before and after exposure to light. Before exposure, Fig. 4 shows two peaks at 577.3 and 579.6 eV, which corresponds to Cr(III) and Cr(VI), respectively.[46] It is evident that, after exposure, the peak for Cr(VI) goes away indicating complete reduction. In addition, we analyzed the solution after regeneration for Cr(VI) content *via* a precipitation of the Cr(III) species using NaOH. After analysis of the remaining supernatant, only a small amount of Cr(VI) remains in the regeneration solution (Fig. S8(c)†). Further, the stability of the Zr-BDC-$(NH_2)_2$ crystals upon Cr(VI) capture and regeneration was confirmed by PXRD (Fig. S5†) and SEM (Fig. S6†). Given the propensity of Zr-MOFs to have defects, the number of missing linkers in this material were also quantified *via* CHN analysis and ICP-OES. On average, ~2 of every 6 BDC-$NH_2$ linkers are missing, which is likely attributed to the etching effect of the acid[47,48] (Table S4†). It should be noted that after long exposure to the HCl solution, ~24 hours, the crystallinity of Zr-BDC-$(NH_2)_2$ is eventually diminished; despite this apparent amorphization, the structure is still intact as proven by FTIR and TGA analyses (Fig. S5†) and the performance remains stable (Fig. S8(a)†). Last, we also performed experiments without light to confirm its impact. The results showed that the adsorption performance remains the same; however, during regeneration, which is carried out in HCl solution and in the dark, only ~55% of the captured Cr is released (Fig. S8†).

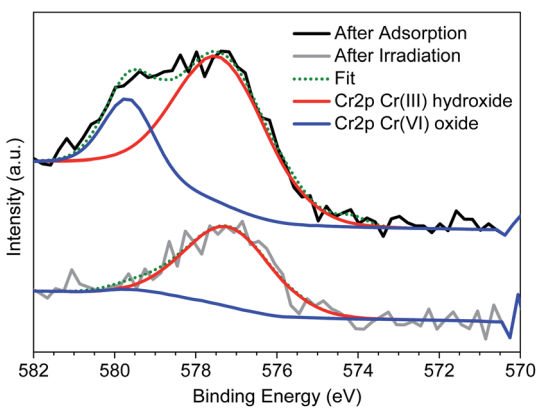


Fig. 4 Cr $2p_{3/2}$ XPS analysis of Zr-BDC-$(NH_2)_2$@PB upon Cr(VI) capture and regeneration.

Given this, it is thought that the reduced Cr(III) species, produced during light regeneration, is more readily released from the sample in acidic media than Cr(VI).

## 5. Capture and photoreduction mechanism

In Scheme 1, the proposed capture and photoreduction mechanism is summarized. Through an ion exchange mechanism, the $Cr_2O_7^{2-}$ anions are exchanged with the two $Cl^-$ ions associated with the protonated $NH_3^+$ functionalities of the ligand of the MOF. This is confirmed by XPS analysis (Fig. S5(d)†). In the regeneration step, the composite is exposed to visible light in a HCl solution. The BDC-$(NH_2)_2$ ligand acts as an antenna to absorb the light and generated photoelectrons can be transferred to the adsorbed $Cr_2O_7^{2-}$, reducing it to Cr(III):

$$Cr_2O_7^{2-} + 14H^+ + 6e^- \rightarrow 2Cr^{3+} + 7H_2O \quad (1)$$

The Cr(III) is released into the solution and the $Cl^-$ ions in the acidic environment reactivate the $NH_3^+Cl^-$ adsorption sites for the next cycle. In the absence of a sacrificial reagent, water accepts the holes and the following photocatalytic redox cycle takes place:

$$h^+ + H_2O \rightleftharpoons OH^\bullet + H^+ \quad (2)$$

The good recyclability of the Zr-BDC-$(NH_2)_2$@PB in combination with their high capacity, fast extraction rate and ability to completely photoreduce Cr(VI) to less toxic Cr(III) makes this composite an outstanding candidate for Cr(VI) extraction–photoreduction.

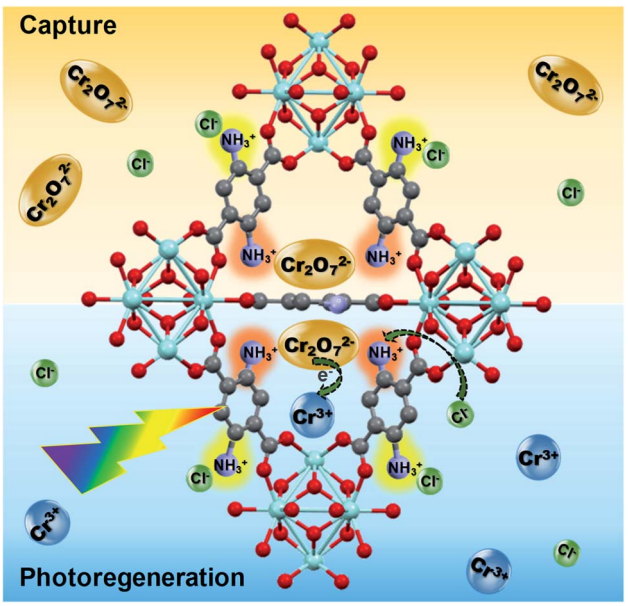


Scheme 1 Schematic representation of capture and photoreduction of Cr(VI).

## 6. Integrated adsorption–photoreduction process

Last, a separation process was developed to demonstrate the viability of the proposed adsorption–photoreduction process. A schematic diagram of the process is shown in Fig. 5, which involves a simple design, that consists of two columns in series. The columns can either be in an extraction or photoregeneration mode by switching the feed from the contaminated water to HCl solution and switching on the light. A $N_2$ flow is bubbled through the column to move the beads and ensure mixing.

It is interesting to compare the design demonstrated here with other technologies reported in the literature. For instance, filtration columns containing MOF powder were previously reported for Cr(VI) capture; however, in these studies sand filtration columns containing only 1–2 wt% of adsorbent were employed.[19,24,30] This is due to the nano/micro-scale MOF particles, which causes difficulties such as clogging, pressure drop, and material loss in liquid-phase adsorption columns. While the sand filler, which offers a larger grain size, helps to avoid these problems, it is thought that this type of technology will lend to large capital costs due to a low volumetric efficiency resulting from large filler to adsorbent ratio. For comparison, Zr-BDC-$(NH_2)_2$ was instead structured into milimeter sized Zr-BDC-$(NH_2)_2$@PB, which can be employed directly in a column without the need for any filler or support. This allows us to take full advantage of the entire column volume. Further, the pressure drop in the system is drastically reduced in comparison to sand filters due to the larger particle size and more efficient packing. While there are several alternative methods to structure MOFs into particles of different shapes and size, these methods often use high pressures, and the resulting MOF particles have diminished properties when compared to their unstructured counterparts.[49,50] The present shaping method leads to minimal loss in MOF surface area, preserves and even enhances the intrinsic properties of the MOF crystals, and provides good mechanical stability to the resulting beads allowing their application in the proposed advanced liquid-phase adsorption system.

For the regeneration process, it is important that the light reaches all the particles in the bed which we achieved by optimizing the $N_2$ flow inside of a transparent glass column (Fig. 5, inset). The column was fed with Cr(VI) solution with a continuous flow of contaminated water having a concentration of 5 ppm Cr(VI). The Cr(VI) concentration was measured at the outlet of each column (Fig. 5). While a single column can successfully remove more than 90% of Cr(VI) over a large operational window, a second column was employed to achieve the EPA drinkable concentration, below 100 ppb. After ~6 hours of adsorption, the Cr(VI) concentration goes above the EPA limit. Next, the columns is regenerated by draining the water and filling the column with HCl solution while irradiating the columns with visible light. To test that all Cr(VI) was converted to

 

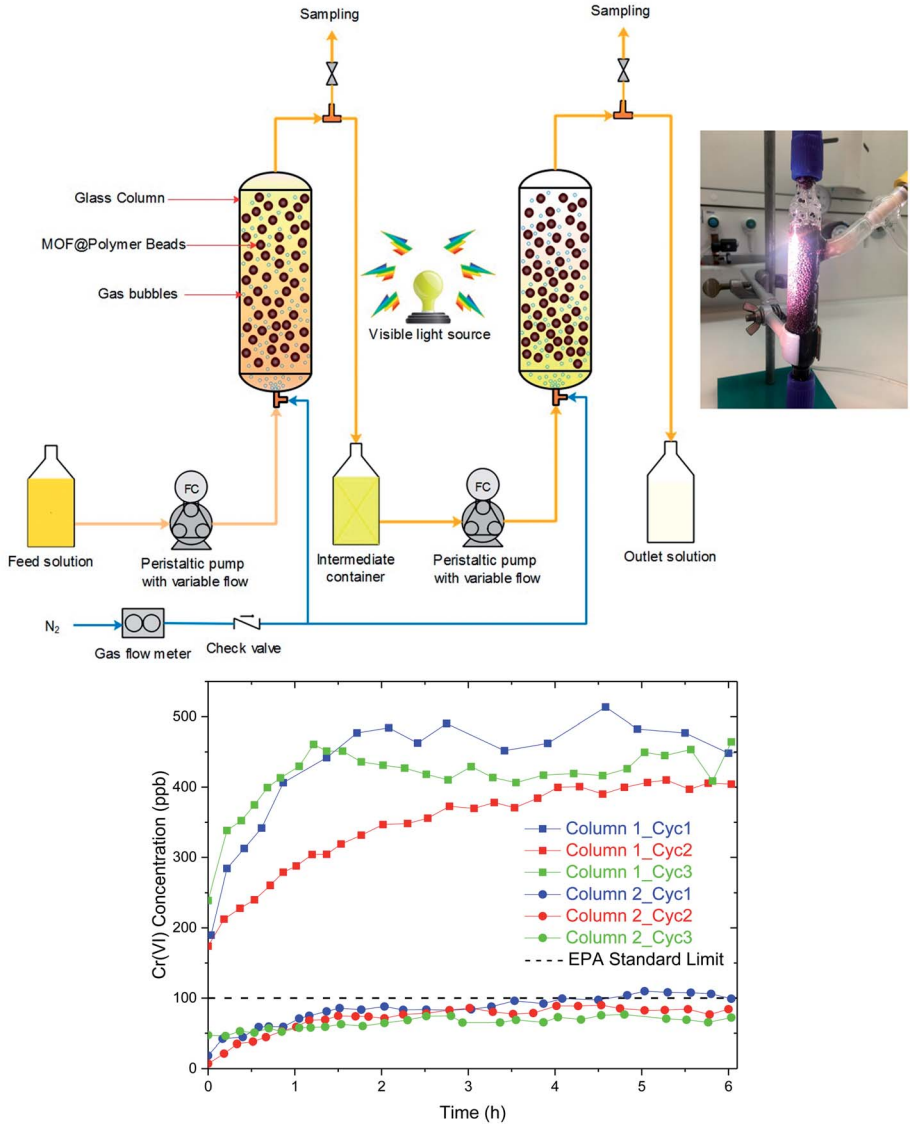


Fig. 5 (Top) The process flow diagram of the gas-sparged adsorption/photoreduction system (inset) column regeneration with HCl solution under irradiation (bottom) Cr(VI) concentration at the outlet of adsorption–photoreduction system (square) column 1 (circle) column 2 for three consecutive cycles.

Cr(III), the Cr(III) species were precipitated from the HCl solution *via* the addition of NaOH and analysis of the supernatant confirms only small amounts of Cr(VI) (Fig. S9†). This regeneration takes ~4 h which is sufficiently shorter than the adsorption window. Hence, a semi-continuous process can be developed by doubling the size of the proposed setup such that one part is in adsorption and the other in the regeneration mode. Three complete cycles were carried out to demonstrate the performance and recyclability of the integrated system. The operation window of 6 h remains effective during three cycles with the final Cr(VI) concentration well below the targeted 100 ppb at the outlet tank.

As a last step, we confirmed the mechanical stability of the composite beads while under continuous flow for extended periods of time. For this, we performed a single column run with gas sparging for the duration of 80 h. After this period, the beads were tested subsequently for Cr(VI) adsorption (Fig. S11†). Despite the bead plasticity, no deformation was observed during the entire process and the adsorption performance remained the same, demonstrating good mechanical stability of the composite beads during process conditions. In addition, the outlet water stream was analyzed for the presence of Zr. Indeed, only trace amounts of the metal, up to 1.72 ppb, was found in the accumulated filtrate solution. This result supports the idea that there are sufficient interactions between the MOF and polymer, which inhibit the loss of Zr-BDC-$(NH_2)_2$ from the bead during the continuous flow process.

# 7. Conclusion

In this work, an integrated adsorption–photoreduction system was developed to capture Cr(VI) in contaminated aqueous solutions and reduce it to Cr(III). To do this, a double amino-functionalized UiO-66 was synthesized and then loaded into chemically modified, hydrophilic polymeric beads, denoted as Zr-BDC-$(NH_2)_2$@PB. The resulting composite simultaneously serves as an adsorbent and photocatalyst and demonstrates one of the highest Cr(VI) uptake capacities reported to date. Additional tests carried out in Rhone river water proves that the composite beads have a high selectivity for Cr(VI) species, even when in the presence of large quantities of other competing cations and anions that are commonly found in surface and ground water. Last, we designed a separation process that has a simple design consisting of two glass columns meant to house the composite beads and an external light source meant to excite the photoactive MOF for the reduction of Cr(VI) to Cr(III). We demonstrate that the system can (i) capture Cr(VI) reducing concentrations to drinkable EPA levels, (ii) reduce the Cr(VI) to the significantly less toxic Cr(III) and (iii) release the Cr(III) for subsequent extraction/regeneration cycles. Because this new method is able to produce only Cr(III) species, it eliminates the need for any post-capture treatment, which is required for the implementation of most adsorbent technologies. To the best of our knowledge, this is the first demonstration of an integrated adsorption–photoreduction system that employs a MOF adsorbent/photocatalyst to capture and reduce Cr(VI) in a single system.

## Conflicts of interest

There are no conflicts to declare.

## Acknowledgements

The authors thank Dr Christopher Patrick Ireland, Dr Natalia Gasilova and Dr Pascal Schouwink for helpful discussions during the preparation of this work and Prof. Mohammad Khaja Nazeeruddin for providing access to his group's infrastructure. B.V. acknowledges the National Center of Competence in Research (NCCR), Materials' Revolution: Computational Design and Discovery of Novel Materials (MARVEL), of the Swiss National Science Foundation (SNSF) for funding (DD4.1 and DD4.5). D.S. acknowledges support of the Swiss National Science Foundation under grant PYAPP2_160581.

## References

1 National Academy of Engineering and National Academies of Sciences, Engineering, Medicine, *Environmental Engineering for the 21st Century: Addressing Grand Challenges*, The National Academies Press, Washington, DC, 2019.
2 K. Kümmerer, D. D. Dionysiou, O. Olsson and D. Fatta-Kassinos, *Science*, 2018, **361**, 222–224.
3 in *The World's Worst Pollution Problems: The Toxics Beneath Our Feet*, Pure Earth and Green Cross Switzerland, 2016.
4 C. B. Klein, *Crit. Rev. Toxicol.*, 2006, **36**, 155–163.
5 S. Lewicki, R. Zdanowski, M. Krzyżowska, A. Lewicka, B. Dębski, M. Niemcewicz and M. Goniewicz, *Ann. Agric. Environ. Med.*, 2014, **21**, 331–335.
6 EPA-USA, in *Chromium in Drinking Water*, https://www.epa.gov/dwstandardsregulations/chromium-drinking-water.
7 in *Toxicological Profile for Chromium*, ed. U.S. Department of Health and Human Services, Agency for Toxic Substances and Disease Registry (ATSDR), Atlanta, Georgia, 2012.
8 in *WHO Guidelines for drinking-water quality; Chromium in drinking-water*, ed. W.H. Organization, WHO/SDE/WSH/03.04/4, Geneva, 2003.
9 C. E. Barrera-Díaz, V. Lugo-Lugo and B. Bilyeu, *J. Hazard. Mater.*, 2012, **223–224**, 1–12.
10 H. Meng, S. Song, S. Lu and A. Lopez-Valdivieso, *Sep. Sci. Technol.*, 2005, **39**, 1501–1517.
11 L. B. Hoch, E. J. Mack, B. W. Hydutsky, J. M. Hershman, J. M. Skluzacek and T. E. Mallouk, *Environ. Sci. Technol.*, 2008, **42**, 2600–2605.
12 C.-C. Wang, X.-D. Du, J. Li, X.-X. Guo, P. Wang and J. Zhang, *Appl. Catal., B*, 2016, **193**, 198–216.
13 P. Kumar, A. Pournara, K.-H. Kim, V. Bansal, S. Rapti and M. J. Manos, *Prog. Mater. Sci.*, 2017, **86**, 25–74.
14 S. Babel and T. A. Kurniawan, *Chemosphere*, 2004, **54**, 951–967.
15 M. Owlad, M. K. Aroua, W. A. W. Daud and S. Baroutian, *Water, Air, Soil Pollut.*, 2009, **200**, 59–77.
16 P. A. Kobielska, A. J. Howarth, O. K. Farha and S. Nayak, *Coord. Chem. Rev.*, 2018, **358**, 92–107.
17 D. T. Sun, L. Peng, W. S. Reeder, S. M. Moosavi, D. Tiana, D. K. Britt, E. Oveisi and W. L. Queen, *ACS Cent. Sci.*, 2018, **4**, 349–356.
18 Q. Zhang, J. Yu, J. Cai, L. Zhang, Y. Cui, Y. Yang, B. Chen and G. Qian, *Chem. Commun.*, 2015, **51**, 14732–14734.
19 S. Rapti, A. Pournara, D. Sarma, I. T. Papadas, G. S. Armatas, Y. S. Hassan, M. H. Alkordi, M. G. Kanatzidis and M. J. Manos, *Inorg. Chem. Front.*, 2016, **3**, 635–644.
20 L.-L. Li, X.-Q. Feng, R.-P. Han, S.-Q. Zang and G. Yang, *J. Hazard. Mater.*, 2017, **321**, 622–628.
21 B. Qiu, C. Xu, D. Sun, Q. Wang, H. Gu, X. Zhang, B. L. Weeks, J. Hopper, T. C. Ho, Z. Guo and S. Wei, *Appl. Surf. Sci.*, 2015, **334**, 7–14.
22 Y. Lai, F. Wang, Y. Zhang, P. Ou, P. Wu, Q. Fang, Z. Chen and S. Li, *Chem. Eng. J.*, 2019, **378**, 122069.
23 T. He, Y.-Z. Zhang, X.-J. Kong, J. Yu, X.-L. Lv, Y. Wu, Z.-J. Guo and J.-R. Li, *ACS Appl. Mater. Interfaces*, 2018, **10**, 16650–16659.
24 W. A. El-Mehalmey, A. H. Ibrahim, A. A. Abugable, M. H. Hassan, R. R. Haikal, S. G. Karakalos, O. Zaki and M. H. Alkordi, *J. Mater. Chem. A*, 2018, **6**, 2742–2751.
25 J. Liu, Y. Ye, X. Sun, B. Liu, G. Li, Z. Liang and Y. Liu, *J. Mater. Chem. A*, 2019, **7**, 16833–16841.
26 S. Kampouri, T. N. Nguyen, C. P. Ireland, B. Valizadeh, F. M. Ebrahim, G. Capano, D. Ongari, A. Mace,

 

N. Guijarro, K. Sivula, A. Sienkiewicz, L. Forró, B. Smit and K. C. Stylianou, *J. Mater. Chem. A*, 2018, **6**, 2476–2481.
27 S. Kampouri, T. N. Nguyen, M. Spodaryk, R. G. Palgrave, A. Züttel, B. Smit and K. C. Stylianou, *Adv. Funct. Mater.*, 2018, **28**, 1806368.
28 L. Shi, T. Wang, H. Zhang, K. Chang, X. Meng, H. Liu and J. Ye, *Adv. Sci.*, 2015, **2**, 1500006.
29 T. N. Nguyen, S. Kampouri, B. Valizadeh, W. Luo, D. Ongari, O. M. Planes, A. Züttel, B. Smit and K. C. Stylianou, *ACS Appl. Mater. Interfaces*, 2018, **10**, 30035–30039.
30 S. Rapti, A. Pournara, D. Sarma, I. T. Papadas, G. S. Armatas, A. C. Tsipis, T. Lazarides, M. G. Kanatzidis and M. J. Manos, *Chem. Sci.*, 2016, **7**, 2427–2436.
31 J. H. Cavka, S. Jakobsen, U. Olsbye, N. Guillou, C. Lamberti, S. Bordiga and K. P. Lillerud, *J. Am. Chem. Soc.*, 2008, **130**, 13850–13851.
32 M. J. Katz, Z. J. Brown, Y. J. Colon, P. W. Siu, K. A. Scheidt, R. Q. Snurr, J. T. Hupp and O. K. Farha, *Chem. Commun.*, 2013, **49**, 9449–9451.
33 H. R. Abid, H. M. Ang and S. Wang, *Nanoscale*, 2012, **4**, 3089–3094.
34 C. Hon Lau, R. Babarao and M. R. Hill, *Chem. Commun.*, 2013, **49**, 3634–3636.
35 B. Valizadeh, T. N. Nguyen, B. Smit and K. C. Stylianou, *Adv. Funct. Mater.*, 2018, **28**, 1801596.
36 E. M. Mahdi, A. K. Chaudhuri and J.-C. Tan, *Mol. Syst. Des. Eng.*, 2016, **1**, 122–131.
37 H. Fei, C. S. Han, J. C. Robins and S. R. J. Oliver, *Chem. Mater.*, 2013, **25**, 647–652.
38 H. Fei, M. R. Bresler and S. R. J. Oliver, *J. Am. Chem. Soc.*, 2011, **133**, 11110–11113.
39 P.-F. Shi, B. Zhao, G. Xiong, Y.-L. Hou and P. Cheng, *Chem. Commun.*, 2012, **48**, 8231–8233.
40 H.-R. Fu, Z.-X. Xu and J. Zhang, *Chem. Mater.*, 2015, **27**, 205–210.
41 X. Li, H. Xu, F. Kong and R. Wang, *Angew. Chem., Int. Ed. Engl.*, 2013, **52**, 13769–13773.
42 B. Ding, C. Guo, S. X. Liu, Y. Cheng, X. X. Wu, X. M. Su, Y. Y. Liu and Y. Li, *RSC Adv.*, 2016, **6**, 33888–33900.
43 B. Ding, J. Z. Huo, Y. Y. Liu, X. Wang, X. Su, X. X. Wu, Z. Z. Zhu and J. Xia, *RSC Adv.*, 2015, **5**, 83415–83426.
44 A. V. Desai, B. Manna, A. Karmakar, A. Sahu and S. K. Ghosh, *Angew. Chem.*, 2016, **128**, 7942–7946.
45 F. Akbal and S. Camcı, *Desalination*, 2011, **269**, 214–222.
46 M. C. Biesinger, B. P. Payne, A. P. Grosvenor, L. W. M. Lau, A. R. Gerson and R. S. C. Smart, *Appl. Surf. Sci.*, 2011, **257**, 2717–2730.
47 Z. Fang, B. Bueken, D. E. De Vos and R. A. Fischer, *Angew. Chem., Int. Ed. Engl.*, 2015, **54**, 7234–7254.
48 J. Koo, I.-C. Hwang, X. Yu, S. Saha, Y. Kim and K. Kim, *Chem. Sci.*, 2017, **8**, 6799–6803.
49 B. Valizadeh, T. N. Nguyen and K. C. Stylianou, *Polyhedron*, 2018, **145**, 1–15.
50 G. W. Peterson, J. B. DeCoste, T. G. Glover, Y. Huang, H. Jasuja and K. S. Walton, *Microporous Mesoporous Mater.*, 2013, **179**, 48–53.